DARU Journal of Pharmaceutical Sciences (2026) 34:47
https://doi.org/10.1007/s40199-026-00625-x

RESEARCH ARTICLE

Novel 3,3′-diindolylmethane derivatives as multi-pathway modulators: targeting estrogen-dependent and independent breast cancer carcinogenesis

Elif Ince-Erguc[1] · Bita Entezari[2,3] · Hanif Sirinzade[4] · Sibel Suzen[5] · Atilla Akdemir[6] · Oguz Erdogan[7] · Hande Gurer-Orhan[3]

Received: 2 April 2026 / Accepted: 28 June 2026

Abstract

Purpose Breast cancer remains a leading cause of cancer-related mortality among women, with prolonged exposure to endogenous estrogens recognized as a major risk factor. This study aimed to design, synthesize, and pharmacologically evaluate novel 3,3′-diindolylmethane (DIM) derivatives as multi-target modulators of estrogen-related pathways in breast cancer.

Methods A series of DIM derivatives was synthesized and structurally characterized. Their biological activities were assessed through aromatase (CYP19A1) and CYP1B1 inhibition assays, E-screen assay for estrogen receptor activity, cytotoxicity assays in breast cancer (MCF-7 BUS, MDA-MB-231) and normal breast epithelial (MCF-10 A) cells, and scratch assay for cell migration. Molecular docking and in silico ADME analyses were conducted to support experimental findings.

Results The derivatives demonstrated significant antiestrogenic activity by targeting multiple components of estrogen signaling. One compound exhibited potent aromatase inhibition (IC_{50} = 0.79 µM), while two derivatives showed strong CYP1B1 inhibition (IC_{50} = 0.37 µM and 0.71 µM). Selective cytotoxicity was observed in estrogen receptor-positive cells, with reduced effects on normal cells. Additionally, selected compounds significantly inhibited cell migration. Molecular modeling revealed favorable binding interactions within target enzymes, and ADME analysis indicated acceptable drug-like properties.

Conclusion These findings suggest that DIM derivatives act as selective, multi-target modulators of estrogen-related pathways and may serve as promising adjuvant candidates for hormone-dependent breast cancer therapy.

Keywords Breast cancer · Aromatase · Estrogen receptor · CYP1B1 · Cytotoxicity · 3,3-Dindolylmethane derivatives

✉ Hande Gurer-Orhan
hande.gurer.orhan@ege.edu.tr

Elif Ince-Erguc
elif.ince@ikcu.edu.tr

Bita Entezari
nina.entez@gmail.com

Hanif Sirinzade
hanif.sirinzade@selcuk.edu.tr

Sibel Suzen
sibel.suzen@pharmacy.ankara.edu.tr

Atilla Akdemir
atilla.akdemir@gmail.com

Oguz Erdogan
oguzerdogan@outlook.com.tr

[1] Department of Pharmaceutical Toxicology, Izmir Kâtip Çelebi University, Izmir, Turkey

[2] Department of Pharmaceutical Toxicology, Istanbul Kent University, Istanbul, Turkey

[3] Department of Pharmaceutical Toxicology, Ege University, Izmir, Turkey

[4] Department of Pharmaceutical Chemistry, Selçuk University, Konya, Turkey

[5] Department of Pharmaceutical Chemistry, Ankara University, Ankara, Turkey

[6] Department of Pharmacology, Istanbul Kent University, Istanbul, Turkey

[7] Department of Drug Discovery and Development, Bezmiâlem Vakıf Üniversitesi, Istanbul, Turkey

Published online: 22 July 2026

Introduction

Breast cancer continues to be a major global health challenge and remains the most commonly diagnosed malignancy among women, has been strongly associated with prolonged exposure to endogenous estrogens. Factors such as early puberty, late menopause, and nulliparity are known to increase breast cancer risk by prolonging estrogen exposure [1, 2]. Estrogen-driven carcinogenesis primarily operates through two mechanisms: the estrogen receptor (ER)-mediated pathway, which promotes cell proliferation via ERα and ERβ, and the receptor-independent pathway, involving the metabolic conversion of estrogens into genotoxic metabolites by enzymes like CYP1B1 [3, 4]. These pathways underscore the importance of targeted interventions in estrogen-driven breast cancer.

CYP19A1, commonly known as aromatase, facilitates the aromatization of androgens into estrogens, serving as a pivotal enzyme in estrogen biosynthesis and the maintenance of hormonal balance. Its overexpression in hormone receptor-positive breast cancers underscores the therapeutic relevance of aromatase inhibition in mitigating estrogen-driven tumor growth [5, 6]. Collectively, these pathways highlight the intricate interplay of molecular mechanisms in estrogen-related breast carcinogenesis and underscore the need for targeted therapeutic interventions (Fig. 1).

The growing interest in natural, diet-derived compounds for cancer prevention and treatment has brought attention to bioactive phytochemicals, particularly those found in cruciferous vegetables like broccoli and cabbage [7–13]. Among these, 3,3'-diindolylmethane (DIM), a metabolite of indole-3-carbinol (I3C), exhibits notable anticancer properties by modulating hormonal balance, reducing oxidative stress, and influencing key signalling pathways [14–17]. DIM has been shown to stimulate the phosphorylation of Brca1 during oxidative stress, playing a protective role against breast cancer [18]. Additionally, DIM sensitizes cells to radiation, inducing apoptosis by arresting the cell cycle at G2/M phase and increasing intracellular ROS generation [19]. Moreover, DIM has been reported to suppress cancer cell migration and invasion, further contributing to its potential in limiting tumor progression and metastasis [20]. DIM has been shown to enhance the efficacy of conventional treatments, such as tamoxifen, while exhibiting favorable safety profiles [21]. However, limitations such as poor stability and low bioavailability hinder its clinical application [22, 23].

To address these challenges, this study synthesized (Scheme 1) and evaluated novel DIM derivatives for their therapeutic potential in breast cancer. Specifically, estrogenic/antiestrogenic potential of the compounds was explored by assessing their ability to inhibit estrogen-induced cell proliferation in MCF-7 BUS cells. Furthermore, the inhibitory effect of the compounds on both aromatase (CYP19A), responsible for local estrogen biosynthesis, and CYP1B1, an enzyme catalysing the bioactivation of various chemicals, including estrogens, into reactive quinone metabolites, was also examined in vitro. Cytotoxicity potentials of the compounds were tested both in human breast cancer and breast epithelial cell lines

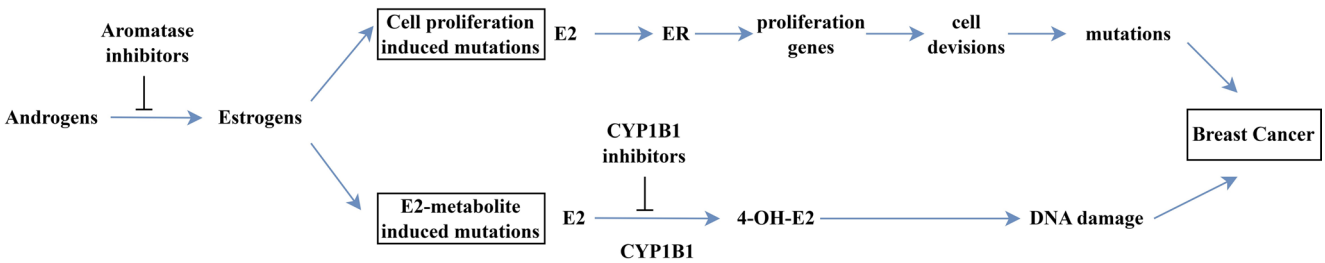

Fig. 1 Estrogen receptor-mediated and estrogen receptor-independent pathways in estrogen-induced carcinogenesis

Scheme 1 Synthesis of DIM derivatives

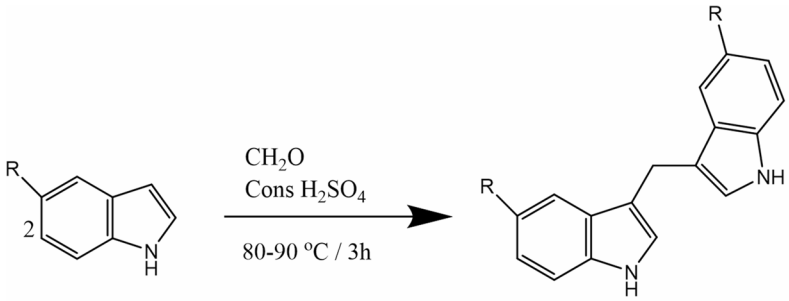

X	R
1	H
2	CN
3	Br
4	Cl
5	F

to check selectivity of the compounds. Additionally, the anti-migratory effects of the compounds were assessed in MCF-7 cells using a scratch assay. Molecular modelling studies of active DIM analogues X2 and X5 with CYP19A1, CYP1B1 and ER was also employed to detect interaction with targets.

Materials and methods

Cell culture and chemicals

MCF-7 BUS cells were kindly provided by Prof. Ana Soto, while MCF-10 A and MDA-MB-231 cells were obtained from ATCC. MCF-10 A cells were cultured in DMEM/F12 supplemented with 5% horse serum, EGF (20 ng/mL), hydrocortisone (0.5 µg/mL), and insulin (10 µg/mL), whereas MCF-7 BUS and MDA-MB-231 cells were maintained in DMEM containing 10% FBS under standard conditions (37 °C, 5% CO_2).

All reagents were purchased from commercial suppliers. The CYP19/MFC assay kit (BD Gentest) and recombinant CYP1B1 enzyme (Corning) were used. Melting points and ESI-MS analyses were performed using standard instrumentation.

General synthesis of DIM derivatives

4 mmol indole/indole derivative was dissolved in 25 mL distilled water, and 2mmol formaldehyde was added to the solution. 2–3 drops of concentrated H_2SO_4 were added dropwise to the mixture and the reaction was stirred at 80–90 °C in a light-free environment for 3 h. The completion of the reaction was checked by TLC. The mixture was allowed to reach room temperature and then the aqueous phase was extracted with diethyl ether 3 times. The extracted organic phases were combined and dried with $MgSO_4$. Finally, the substance obtained by evaporating diethyl ether in the evaporator was recrystallized with ethyl alcohol to obtain the pure compound [24]. As a result, compounds X1–X5 were obtained in yields of 40%, 47%, 30%, 33%, and 35%, respectively.

Aromatase activity assay

Aromatase inhibitory effects of synthesized DIM derivatives were evaluated by using CYP19/MFC High throughput Screening Kit supplied from BD Gentest. Assay was performed according to the previous study [25]. Aromatase inhibitory effects of DIM derivatives were evaluated in different concentrations (0.045-100 µM), inhibition curves were assessed and IC_{50} values were calculated for each compound.

Ethoxy resorufin-O-dealkylation (EROD) assay

This assay is based on dealkylation reaction of 7-ethoxyresorufin by CYP1 (CYP1A1, CYP1A2 and/ or CYP1B1) enzymes and formation of its fluorescent resorufin metabolite [26]. Firstly, IC_{50} values of DIM derivatives for CYP1 inhibition were assessed by using phenobarbital induced rat liver microsomal CYP1 enzymes. To evaluate CYP1 inhibitory effect of compounds 10 µL microsome, 90 mM KH_2PO_4/K_2HPO_4 (pH 7.4), 3.7 µM 7-ethoxyresorufin, different concentrations of test compound and 0.22 mM NADPH with the final volume of 250 µL were added to tubes, respectively, incubated at 30 °C for 10 min and the reaction was stopped by adding 500 µL acetone to each tube, centrifuged at 12,500 g (4 °C) for 5 min and the fluorescence intensity of the supernatants were measured at 530 nm (excitation) and 586 nm (emission). Inhibitory effects of potent inhibitors of CYP1, were further assessed by human recombinant CYP1B1 enzyme. After the addition of 1.25 pmol enzyme, 0.2 µM substrate and test compound the method was performed at 37 °C as described above.

E-screen assay

The E-screen method developed for the evaluation of estrogen receptor (ER)-mediated effects of chemicals was used in this study [27]. Compounds with estrogenic activity bind to ER and induce the MCF-7 BUS cell proliferation in a hormone free media, on the contrary, antiestrogenic compounds inhibit the cell proliferation, in the presence of estradiol by blocking ER. This assay was performed as described previously [28]. Briefly, to evaluate estrogenic activity, MCF-7 BUS cells were treated with 1.1 µM of DIM derivatives in a hormone free media (phenol red free DMEM supplemented with 10% Charcoal Dextran FBS, 1% MEM-NAA, 1% Sodium pyruvate) for 144 h. Besides, antiestrogenic activities were assessed by adding 10^{-10} M estradiol to each well as well as the test compound. The tested concentration was selected to minimize cytotoxic interference during evaluation of antiestrogenic activity. At the end of the incubation period cells were fixed with 10% trichloroacetic acid (TCA), stained with 0.4% sulforhodamine B (SRB) solution and optical densities were measured at 492 nm by Themo Scientific Varioscan Flash (U.S.) multiplate reader.

Cell viability

Cell viability was assessed using the MTT assay to evaluate the effects of DIM derivatives on MCF-10 A, MCF-7 BUS and MDA-MB-231 cell viability was evaluated with MTT assay. This assay is based on the ability of mitochondrial dehydrogenases in viable cells to reduce MTT (3-(4,5-dimethylthiazol-2-yl)-2,5-diphenyltetrazolium bromide) into insoluble purple formazan crystals [29]. Briefly, cells were seeded at a density of 6000 cells per well and incubated for 24 h at 37 °C. Subsequently, cells were treated with varying concentrations of DIM derivatives or paclitaxel as a positive control for 48 h. Following treatment, wells were washed with phosphate buffered saline (PBS) and incubated with MTT solution for 2 h at 37 °C. The media was then removed, and the formed formazan crystals were solubilized in DMSO. Absorbance was measured at 550 nm using a multiplate reader.

Scratch assay

Cell migration was evaluated using a scratch (wound healing) assay. MCF-7 cells were seeded in 12-well plates (2.5×10^5 cells/well) and incubated for 24 h. A scratch was created, and cells were treated with compounds at their IC_{20} concentrations in DMEM containing 1% FBS. Images were captured immediately after treatment (0 h) and after 24 h incubation using a light microscope at 4× magnification. Scratch widths were quantified using ImageJ software, and the closure rate and percentage of cell migration were calculated relative to the vehicle control.

In silico ADME prediction

The pharmacokinetic properties of the DIM derivatives were predicted using the web-based tool SwissADME. The canonical SMILES of each compound were obtained and submitted to the platform for analysis. Key parameters evaluated included physicochemical properties (e.g., molecular weight, lipophilicity), water solubility, gastrointestinal absorption, blood–brain barrier permeability, and drug-likeness according to established rules (Lipinski). Additionally, potential interactions with cytochrome P450 isoenzymes and P-glycoprotein substrate status were assessed. All predictions were performed using the default settings of the platform.

Molecular modelling studies

The Schrödinger software package (v2023–4, Schrödinger, Inc., New York) was used for the molecular modelling studies.

Protein preparation

The crystal structure of CYP19A1 in complex with 4-androstene-3-17-dione (PDB: 3S79; 2.75 Å), Estrogen receptor in complex with the ligand OP107 (PDB: 5UFX; 1.55 Å), Estrogen receptor in complex with estradiol (PDB: 5DXE; 1.50 Å) and CYP1B1 in complex with the 2-phenyl-4 H-benzo[H]chromen-4-one (PDB: 3PM0; 2.70 Å) were downloaded from the Protein Data Bank. Protein and ligand atoms were retained while all water molecules and sulfate ions were deleted. The Protein Preparation Wizard module was used to prepare the protein structure, which was pre-processed by adding hydrogens and missing side chains if present. The N- and C-terminals of the proteins were capped and subsequently, the system was minimized using the OPLS4 force field.

Docking

A grid file was generated using the Receptor Grid Generation tool. The grid was prepared around the centroid of the co-crystallized ligand. All hydroxyl groups of the Ser, Thr and Tyr residues that were lining the binding pocket and not forming hydrogen bonding interactions with other amino acids were allowed to rotate during dockings. The three-dimensional structures of compounds X2 and X5 were prepared with the Builder and LigPrep tools. Subsequently, the compound was docked into the binding pocket using the Glide tool and Extra Precision (XP) scoring function with default settings. The highest scoring three poses were retained and investigated for complementarity in shape, hydrogen bonding characteristics, electrostatics and hydrophobicity between ligand and binding pocket.

Molecular dynamics simulations

All molecular dynamics (MD) simulations were conducted using the Desmond software package. The selected ligand–receptor complexes were positioned centrally within an orthorhombic simulation box, applying periodic boundary conditions and ensuring at least a 10 Å buffer between the protein surface and box edges. To establish a neutral and solvated environment, water molecules modeled with the TIP5P model and 0.15 M NaCl were introduced. Energy minimization was performed for 100 ps using the OPLS4 force field, maintaining positional restraints on the protein and ligand atoms. Subsequent MD simulations were executed for 250 ns

under NPT ensemble conditions, maintaining temperature at 300 K (Nose–Hoover thermostat) and pressure at 1 bar (Martyna–Tobias–Klein barostat), utilizing the RESPA integrator with a 2 fs time step and no restraints. The trajectory data were analyzed using the Simulation Interaction Diagram tool to monitor Cα atom RMSD and ligand–protein interactions throughout the simulation period. Additionally, MM-GBSA binding free energy calculations were performed using the thermal_MMGBSA.py script to estimate the stability of the complexes during the 250 ns trajectory [30].

Statistical analysis

Data were analysed in GraphPad Prism 8 and expressed as means ± SD. Statistical analysis was performed by using one-way ANOVA test and then Tukey's or Dunnett's test was applied as a post hoc test. Differences were considered significant in case of $p < 0.05$. Statistical significance is expressed as $p < 0.05$*, $p < 0.01$**, $p < 0.001$***.

Results and discussion

In recent years, a growing body of literature has highlighted the potential of diet-derived chemopreventive agents in cancer prevention and therapy [31–35]. Notably, bioactive compounds found in cruciferous vegetables, such as Brussels sprouts, broccoli, and cabbage, have garnered significant attention due to their promising anticancer properties [36, 37]. However, the consumption of these compounds through whole foods poses challenges, including the inability to standardize dosage and the difficulty in conducting comprehensive safety assessments. Consequently, the synthetic production of these active secondary metabolites such as indoles, indole-3-carbinol (I3C) and its active metabolite 3,3′-diindolylmethane (DIM) can offer a viable alternative, enabling precise dose standardization, enhanced therapeutic efficacy, and rigorous safety evaluation for potential use as targeted chemopreventive agents.

Within this context, the present study focuses on the development and evaluation of novel DIM-based derivatives. A set of five compounds was generated and subjected to structural confirmation, followed by a systematic investigation of their biological activities across multiple breast cell models. Their effects were examined not only in estrogen-dependent breast cancer cells but also in normal breast epithelial and triple-negative breast cancer cells, enabling a comparative assessment of their selectivity and functional relevance.

Chemical characterisation of the synthesised DIM derivatives

3,3'-Methanediylbis(1H-indole) X1: **^{1}H-NMR (500 MHz, $CDCl_3$, δ)**: 4.26 (s, 2H, CH_2), 6.93 (t, 2H, J = 1.2 Hz, H-2,2'), 7.11 (td, 2 H, J_O=7.6 Hz, J_m=0.8 Hz, H-5,5'), 7.21 (td, 2 H, J_O=7.2 Hz, J_m=1.2 Hz, H-6,6'), 7.36 (d, 2 H, J_O=8.4, H-7,7'), 7.64 (d, 2 H, J_O=7.6, H-4,4'), 7.87 (s, 2 H, indole-NH). **^{13}C-NMR (125 MHz, $CDCl_3$, δ)**: 21.2, 111.1, 115.7, 119.9, 119.2, 121.9, 122.2, 127.6, 136.4. LRMS (ESI, positive) m/z calcd for $C_{17}H_{14}N_2$ $[M]^+$: 247.04, found: 247.05, $[M+H]^+$: 248.01. Yield: 40%, m.p: 167 °C.

3,3'-Methanediylbis(1H-indole-5-carbonitrile) X2: **^{1}H-NMR (500 MHz, DMSO, δ)**: 4.20 (s, 2H, CH_2), 7.37 (dd, 2H, J_o=8.4 Hz, J_m=1.6 Hz, H-6,6'), 7.47–7.49 (m, 4 H, Ar-H), 8.07 (s, 2 H, H-2,2'), 11.39 (s, 2 H, indole-NH). **^{13}C-NMR (125 MHz, DMSO-d_6, δ)**: 20.1, 100.9, 112.7, 115.0, 120.9, 123.6, 124,4, 125.7, 126.9, 138.1. LRMS (ESI, positive) m/z calcd for $C_{19}H_{14}N_4$ [M]$^+$: 298.12, found: 298.15, $[M+H]^+$: 299.10. Yield: 47%, m.p: 141–142 °C.

3,3'-Methanediylbis(5-bromo-1H-indole) X3: **^{1}H-NMR (500 MHz, DMSO, δ)**: 4.14 (s, 2H, CH_2), 6.95 (t, 2H, J = 1.2 Hz, H-2,2'), 7.22–7.29 (m, 4 H, Ar-H), 7.71 (d, 2 H, J_m=0.88, H-4,4'), 7.97 (s, 2 H, indole-NH). **^{13}C-NMR (125 MHz, $CDCl_3$, δ)**: 21.1, 112.6, 114.9, 121.8, 123.4, 124.9, 129.2, 135.1. LRMS (ESI, positive) m/z calcd for $C_{17}H_{14}Br_2N_2$ $[M]^+$: 403.95, found: 403.90, $[M+H]^+$: 404.10. Yield: 30%, m.p: 172–173 °C.

3,3'-Methanediylbis(5-chloro-1H-indole) X4: **^{1}H-NMR (500 MHz, DMSO, δ)**: 4.17 (s, 2H, CH_2), 7.00 (t, 2H, J = 0.88 Hz, H-2,2'), 7.16 (dd, 2 H, J_o=5.6 Hz, J_m=1.6 Hz, H-6,6'), 7.30 (d, 2 H, J_O=6.92, H-7,7'), 7.57 (d, 2 H, J_m=1.6, H-4,4'), 7.98 (s, 2 H, indole-NH). **^{13}C-NMR (125 MHz, $CDCl_3$, δ)**: 21.1, 112.1, 115.0, 118.7, 122.3, 123.6, 125.0, 128.5, 134.8. LRMS (ESI, positive) m/z calcd for $C_{17}H_{14}Cl_2N_2$ $[M]^+$: 316.05, found: 316.09, $[M+H]^+$: 317.07. Yield: 33%, m.p: 148–150 °C.

3,3'-Methanediylbis(5-fluoro-1 H-indole) X5: **^{1} H-NMR (500 MHz, DMSO, δ)**: 4.17 (s, 2 H, CH2), 6.95 (td, *J* = 9.0, 2.5 Hz, 2 H), 7.03 (dd, *J* = 2.3, 1.2 Hz, 2 H), 7.23 (dd, 2 H), 4.17 (s, 2 H). 7.29 (dd, *J* = 8.8, 4.2, 0.5 Hz, 2 H), 7.95 (s, 2 H, indole-NH). **^{13}C-NMR (125 MHz, $CDCl_3$, δ)**: 21.2, 104.0, 104.2, 110.2, 110.5, 111.6, 111.70, 115.4, 115.5, 123.9, 127.8, 127.9, 133.0, 156.7, 158.6. LRMS (ESI, positive) m/z calcd for $C_{17}H_{14}F_2N_2$ $[M]^+$: 284.11, found: 284.13, $[M+H]^+$: 285.23. Yield: 35%, m.p: 144 °C.

Aromatase (CYP19A1) inhibitory effects

Aromatase, a crucial enzyme in estrogen biosynthesis, catalyze the conversion of androgens to estrogens and contributes to maintaining estrogenic balance within the body. Inhibition of aromatase has emerged as a significant therapeutic strategy in breast cancer management, aiming to mitigate the estrogenic drive fueling tumor growth. The potential aromatase inhibitory effects of DIM derivatives were initially screened at a concentration of 100 µM using a fluorescent substrate (MFC) and a human recombinant aromatase enzyme in an in vitro cell free assay. All compounds were found to significantly inhibit aromatase activity (data not shown). The inhibitory effects of each compound were further analysed at different concentrations and IC_{50} values were calculated to determine the potency of the DIM derivatives (Table 1). All tested derivatives inhibited enzyme activity in a dose-dependent manner, with compound X2 being the most potent, exhibiting an IC_{50} value of 0.79 µM. The inhibition curves of compounds are given as supplementary data (Supporting information Fig.S16).

In line with previous findings demonstrating that DIM suppresses aromatase expression in estrogen-dependent breast cancer cells (MCF-7), functioning as an aromatase inhibitor [38], our study showed that specific DIM derivatives significantly inhibited aromatase activity, with IC_{50} values in the low micromolar range Comparing IC_{50} values only compound X2 (IC_{50}: 0.79 µM) inhibited aromatase enzyme with lower IC_{50} value than DIM (nonsubstituted; X1). This value was comparable to the first-generation aromatase inhibitor aminoglutethimide (IC_{50}: 0.6 µM) [39]. However, its inhibitory potency was notably lower when compared to the third-generation aromatase inhibitor letrozole, with an IC_{50} value of 4 nM [40].

Table 1 IC_{50} values of DIM derivatives against human recombinant CYP19A1, CYP1 (microsomes) and human recombinant CYP1B1 activity. IC_{50} values were determined by nonlinear regression analysis of dose–response curves generated from triplicate measurements; values in parentheses indicate 95% confidence intervals. AG: aminoglutethimide, KTZ: Ketoconazole

DIM derivatives	IC_{50} (µM) [95% CI]		
	CYP19A1	**Microsomal CYP1**	**CYP1B1**
X1(DIM)	10.76(7.8–14.8)	1.92 (1.3–2.8)	-
X2	0.79(0.7–0.8)	0.23 (0.1–0.4)	0.37(0.1–0.7)
X3	35.8(19.5–65.7)	0.57 (0.3–0.9)	-
X4	23.8(10.3–54.8)	1.86 (1.1-3)	-
X5	12.3(8.5–17.8)	0.19 (0.09–0.3)	0.71(0.3-1)
AG	0.38(0.3–0.4)	-	-
KTZ	2.3(1.8–2.8)	1.7 (1.2–2.4)	3.1 (2.3–3.9)

CYP1B1 inhibitory effects

CYP1B1, a member of the Cytochrome P450 1 family, an enzyme involved in phase I drug metabolism and bioactivation of various procarcinogens, primarily acts as a hydroxylase for 17β-estradiol [41]. Elevated expression of CYP1B1 is found in various tumors, especially hormone-related cancers like breast, ovary and prostate, suggesting its involvement in cancer progression [42, 43]. Studies indicate that multiple hallmarks of breast cancer progression, including cell proliferation, invasion, and migration, were increased following CYP1B1 induction [44]. Moreover as an enzyme that contributes to the metabolic activation of estrogens and xenoestrogens, the inhibition of CYP1B1 emerges as a prospective strategy to impede the formation of genotoxic metabolites and, consequently, mitigate the risk of breast cancer initiation and progression [45]. In this study the potential CYP1 inhibitory effects of DIM derivatives were analysed in microsomes by using 7-ethoxyresorufin as a substrate. All the compounds significantly and dose dependently inhibited CYP1 enzymes (Supporting information Fig. S17). X2 and X5 were found to inhibit microsomal CYP1 activity more potently with IC_{50} values of 0.23 and 0.19 µM, respectively (Table 1). Accordingly, inhibitory effects of these two compounds were further tested on human recombinant CYP1B1 enzyme (Supporting information Fig.S18). Both compounds were shown to be the potent inhibitors of CYP1B1 with IC_{50} values of 0.37 µM (X2) and 0.71 µM (X5). The relatively higher IC_{50} values observed in the microsomal CYP1 assay compared to recombinant CYP1B1 may be associated with differential inhibitory effects of these compounds on other CYP1 isoforms, including CYP1A1 and CYP1A2. Therefore, further studies are required to clarify CYP isoform selectivity. Dutour and Poirier have reviewed wide variety of natural compounds that inhibit CYP1B1 enzyme [46]. Some compounds, particularly those with a stilbene structure, inhibited the CYP1B1 enzyme at nanomolar concentrations, indicating that X compounds (DIM derivatives) may not be the optimal candidates for CYP1B1 inhibition. On the other hand, compound X2 and X5 exhibited greater potency in inhibiting CYP1B1 compared to a flavonoid compound (IC_{50}: 43 µM) and purpurin (IC_{50}: 2.2 µM). Previous studies demonstrated that treatment with cabbage juices or I3C/DIM led to a reduction in CYP1B1 expression in MCF-7

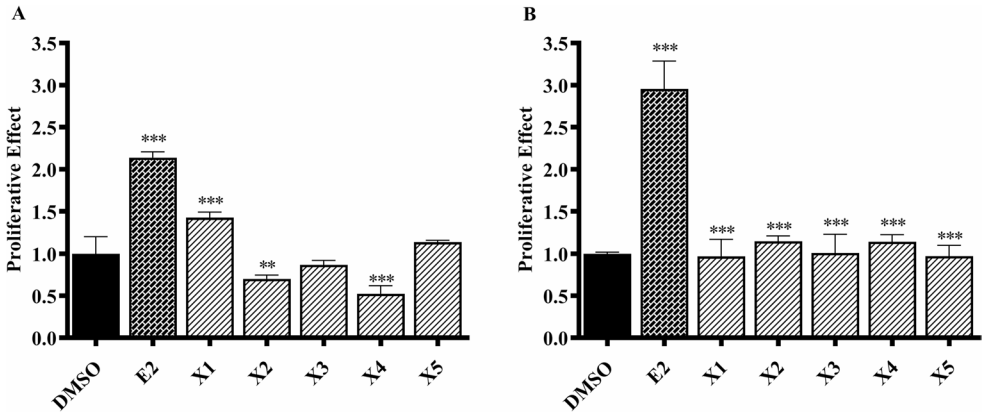

Fig. 2 Estrogenic (**A**) and antiestrogenic (**B**) effects of DIM derivatives (1.1µM) in MCF-7 cells. Statistical analyses were performed by comparing samples with DMSO for estrogenic activity and with E2 group for antiestrogenic activity. DMSO: Dimethyl sulfoxide; E2: Estradiol. *$p<0.05$, **$p<0.01$, ***$p<0.001$

cells [47]. In the current study, DIM derivatives (specifically X2 and X5) exhibited a stronger inhibitory effect compared to DIM (X1). These findings suggest that the compounds may modulate estrogen metabolism through CYP-related pathways, potentially reducing the formation of genotoxic estrogen metabolites associated with breast carcinogenesis.

Estrogen receptor mediated effects

Numerous studies have demonstrated that I3C or its analogues possess the ability to bind to ER and act as either estrogenic or antiestrogenic activity [48]. The effects of the DIM derivatives on estrogen receptor were investigated using the E-screen assay. To assess estrogenic effects, cells were incubated with the test substances in estrogen-free media, and proliferative effects (PE) were calculated for each compound. Among the compounds only X1 increased cell proliferation, with a PE value of 1.49 (Fig. 2A). Previous studies reported that physiologically obtainable concentrations of DIM, specifically at 10 µM, activated the ERα signalling pathway which stimulate cell proliferation in MCF-7 cell line [49]. Our results confirmed this finding, as the non-substituted compound X1 (DIM) induced cell proliferation in the absence of estradiol (Fig. 2A), suggesting an estrogenic activity. In contrast, PE values for X2 and X4 were below 1, suggesting potential antiestrogenic activity. Subsequently, the antiestrogenic effects of the compounds were evaluated in the presence of 0.1 nM estradiol and 1.1 µM of each test substance. All derivatives significantly inhibited MCF-7 BUS cell proliferation, even in the presence of estradiol in the media (Fig. 2B). The PE values for X1, X2, X3, X4 and X5 were calculated as 0.97, 1.15, 1, 1.14 and 0.96, respectively, suggesting potential antiestrogenic effects of the newly synthesized DIM derivatives.

Effects on cell viability

The cytotoxic effects of the DIM derivatives were evaluated in MCF-7 BUS, MDA-MB-231, and MCF-10 A cells following 48 h treatment (Table 2). Compared to the parent compound DIM (X1), which exhibited weak activity in MCF-7 BUS cells (IC_{50} = 95 µM), all substituted derivatives showed markedly enhanced cytotoxicity. In particular, X3 and X4 demonstrated the highest potency in MCF-7 BUS cells, with IC_{50} values of 21.5 µM and 22 µM, respectively, followed by X2 (28.3 µM) and X5 (46 µM), indicating that structural modification of the DIM scaffold significantly improves anticancer activity.

A similar but less pronounced trend was observed in MDA-MB-231 cells, where X3 and X4 exhibited IC_{50} values of 30.4 µM and 31.5 µM, respectively. Overall, the compounds displayed greater cytotoxic potency in MCF-7 BUS cells compared to MDA-MB-231 cells, suggesting a higher sensitivity of estrogen receptor-positive breast cancer cells to these derivatives. This observation is consistent with previous studies reporting that ERα-positive breast cancer cells are more responsive to DIM-based compounds than ER-negative cells [50].

Importantly, all compounds showed higher IC_{50} values in MCF-10 A cells (33–44 µM) than in MCF-7 cells, indicating lower cytotoxicity toward normal breast epithelial cells.

Table 2 IC_{50} values of DIM derivatives

DIM derivatives	IC_{50} (µM)		
	MCF-7 BUS	**MDA-MB-231**	**MCF-10A**
X1	95	> 100	> 100
X2	28.3	36.3	34
X3	21.5	30.4	44
X4	22	31.5	33
X5	46	44.5	39
Paclitaxel	0.035	0.076	0.29

Notably, DIM (X1) exhibited minimal cytotoxicity in both MDA-MB-231 and MCF-10 A cells (IC_{50} >100 µM), further highlighting the improved activity achieved through structural modification. Although the observed selectivity was moderate, the compounds generally displayed greater cytotoxic activity in ER-positive MCF-7 cells than in normal breast epithelial cells. This trend is consistent with previous reports showing that DIM derivatives may exhibit preferential activity toward cancer cells relative to non-transformed cells [51].

The reduced efficacy observed in MDA-MB-231 cells further supports the role of estrogen receptor-mediated mechanisms in the activity of these compounds, as also reported in the literature. In this context, alternative pathways such as AMPK activation may be explored to enhance activity in triple-negative breast cancer models [52].

Despite these promising findings, the cytotoxic potency of the DIM derivatives remained substantially lower than that of paclitaxel (IC_{50} = 0.035 µM in MCF-7 BUS), indicating that these compounds are unlikely to serve as direct alternatives to conventional chemotherapeutics. However, their moderate cytotoxicity, combined with selective activity toward cancer cells and their ability to modulate multiple targets, including aromatase, CYP1B1, and cell migration, suggests that they may represent promising candidates as adjuvant or multi-target agents in breast cancer therapy.

In addition to their direct cytotoxic effects, DIM derivatives may also possess chemosensitization potential, particularly in overcoming chemoresistance, as previously reported for structurally related indole derivatives [53, 54]. Further studies investigating combination treatments with conventional chemotherapeutics such as docetaxel are warranted.

Effects on cell migration

The anti-migratory effects of the compounds were assessed in MCF-7 cells at their IC_{20} concentrations using a scratch (wound healing) assay, as these cells exhibited higher sensitivity to the compounds compared to MDA-MB-231 cells. As shown in Fig. 3 compounds X1, X4, and X5 significantly reduced cell migration compared to the vehicle control ($p < 0.05$), decreasing migration by 19%, 24%, and 25%, respectively, indicating that X4 and X5 exhibit stronger anti-migratory effects than the parent DIM compound (X1). These findings are consistent with previous reports on DIM, indicating that the anti-migratory effects may be linked to the modulation of estrogen-related pathways, particularly through aromatase and CYP1B1 inhibition [20].

In silico ADME prediction

The pharmacokinetic properties and drug-likeness of the synthesized DIM derivatives (X1–X5) were evaluated using the SwissADME platform (Table 3). All compounds exhibited molecular weights within the acceptable range (246.31–404.10 g/mol) and complied with Lipinski's rule of five, with the exception of X3, supporting their oral drug-likeness. The derivatives demonstrated balanced lipophilicity (iLogP: 0–2.87; MLogP: 2.13–4.23) and low TPSA values (31.58 Å² for most compounds), indicating favorable membrane permeability, which is consistent with their observed biological activity.

All compounds were predicted to have high gastrointestinal absorption, while most derivatives (X1, X3, X4, and X5) also showed blood–brain barrier permeability. The identification of all compounds as P-glycoprotein substrates suggests potential efflux-related limitations in bioavailability. The predicted CYP inhibition profile revealed interactions with key isoforms, including CYP1A2, CYP2D6, and CYP3A4, which may contribute to their multi-target activity. Notably, this profile aligns with the experimentally observed inhibition of CYP1B1, supporting the role of these compounds in modulating estrogen-related metabolic pathways.

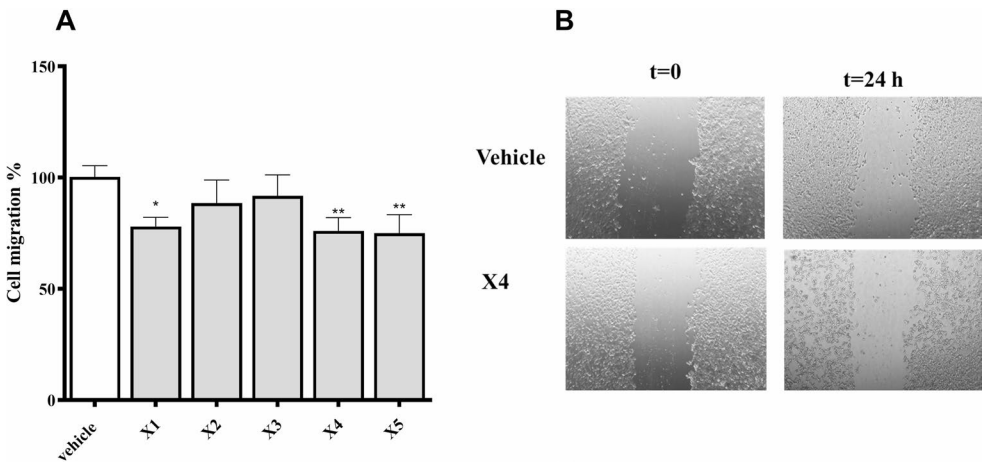

Fig. 3 The effects of compounds on cell movement in MCF-7 cells were evaluated using the scratch assay. (**A**) Representative images were obtained from the same wells at 0 h and after 24 h of incubation. (**B**) Cell migration was quantified as the percentage of wound closure relative to the vehicle-treated control, which was normalized to 100%. Data are presented as mean ± SD ($n = 3$ independent experiments, $N = 3$ wells per experiment). Statistical significance was determined relative to the vehicle control (*$p < 0.05$, **$p < 0.01$)

Table 3 Physicochemical properties and ADME predictions of DIM derivatives based on Swiss ADME analysis

Predicted parameters	Compounds				
	X1	**X2**	**X3**	**X4**	**X5**
MW (g/mol)	246.31	298.34	404.10	315.20	282.29
NHD	2	2	2	2	2
NHA	0	2	0	0	2
NRB	2	2	2	2	2
TPSA (A^{o2})	31.58	79.16	31.58	31.58	31.58
iLogP lipophilicity	1.99	0	2.87	2.69	2.28
MLogP lipophilicity	3.00	2.13	4.23	4.00	3.77
LogS (ESOL) water solubility	-4.52	-4.36	-6.30	-5.67	-4.80
Lipinski's violation	0	0	1	0	0
ADME predictions					
GI absorption	High	High	High	High	High
BBB permeability	Yes	No	Yes	Yes	Yes
P-gp substrate	Yes	Yes	Yes	Yes	Yes
CYP inhibition					
CYP1A2	Yes	Yes	Yes	Yes	Yes
CYP2C19	Yes	No	Yes	Yes	Yes
CYP2C9	No	No	No	No	No
CYP2D6	Yes	Yes	Yes	Yes	Yes
CYP3A4	Yes	Yes	Yes	Yes	Yes

NHD number of hydrogen donors, *NHA* number of hydrogen acceptors, *NRB* number of rotatable bonds, and *TPSA* total polar surface area, *GI* gastrointestinal, *BBB* blood brain barrier, *P-gp* P-glycoprotein, and *CYP* cytochrome

Overall, X4, and X5 exhibited the most favorable balance of physicochemical and pharmacokinetic properties, which, together with their selective cytotoxicity and anti-migratory effects, highlights their potential as multi-target agents for breast cancer therapy. However, these findings are based on in silico predictions, and further experimental studies are required to confirm the physicochemical and pharmacokinetic properties of the compounds.

Molecular modelling studies

Molecular modelling studies were performed to investigate the binding interactions of compounds X2 and X5 with CYP19A1 and CYP1B1. To this end, compounds X2 and X5 were docked into crystal structures of CYP19A1 and CYP 1B1.

Interactions with aromatase (CYP19A1)

Compound X2 formed a hydrogen bond between the nitrile group of the ligand and the backbone of Leu372. In addition, a π-π interaction with Trp224 and a cation-π interaction with the haem group were formed (Fig. 4A, B). A 250 ns MD simulation indicates that the binding interactions of the ligand with the aromatase active site changes. The MD simulation revealed that the ligand adopted another pose in the binding pocket as the RMSD value increased towards approximately 3.5–4.5 Å (Fig. 4D). The observed hydrogen bond with Leu372 was not preserved during the simulation and a new hydrogen bond was formed water-mediated hydrogen bond with Gln367 (33% of simulation time) and Pro368 (33% of simulation time). In the other side a new hydrogen bond was formed with the side chain of Met374(98% of simulation time) (Fig. 4C). In addition, water-mediated hydrogen bonds were observed with backbone of Ala306 (56% of simulation time). The MM/GBSA binding energy (kcal/mol) was mainly between −30 and −50 kcal/mol (Fig. 4E). The average binding energy was −39,1060+/- 6,6998 kcal/mol.

Compound X5 formed a hydrogen bond between one of its amine groups and the backbone carbonyl group of Leu477 and an aromatic hydrogen bond with the side chain of Asp309 (Fig. 4F, G). One of its indole groups formed a π-π stacking with the side chain of Trp224. A fluor atom was at 2.51 Å distance from the cationic side chain of Arg115 and as such may form electrostatic interactions. A 250 ns MD simulation indicates that the binding interactions of the ligand with the aromatase active site changes. During the first 115 ns of the simulation, the ligand RMSD value increased towards approximately 3.5–4.0 Å. Afterwards, the RMSD value increased towards approximately 5.6–6.4 Å (Fig. 4I). During the first part of the MD simulation (0–115 ns), one of the indole rings of the ligand formed π-π stackings with the side chains of Phe221 (61% of simulation time) and Trp224 (79% of simulation time), while the other indole ring was involved in a hydrogen bond with Leu372 (92% of simulation time) (Fig. 4H). After this period (115–250 ns), mainly hydrophobic interactions were observed. The MM/GBSA binding energy (kcal/mol) was mainly between −20 and −40 kcal/mol, except in the first part of the simulation (0–10 ns) and around 110 ns (Fig. 4J). The average binding energy was −28.0866 +/- 7,5681 kcal/mol.

Interactions with human CYP1B1

The docked pose of X2 showed that one of the indole rings was located close to the haem group and formed π-π stack interactions with the haem group and Phe134 (Fig. 5A, B). The other indole ring formed π-π stacking with the sidechain of Phe231. During the MD simulation the ligand's RMSD value increased towards approximately 2–2.5 Å (Fig. 5D), indicating a change in binding interactions. One of the indole rings preserved π-π stack interactions with the sidechain of

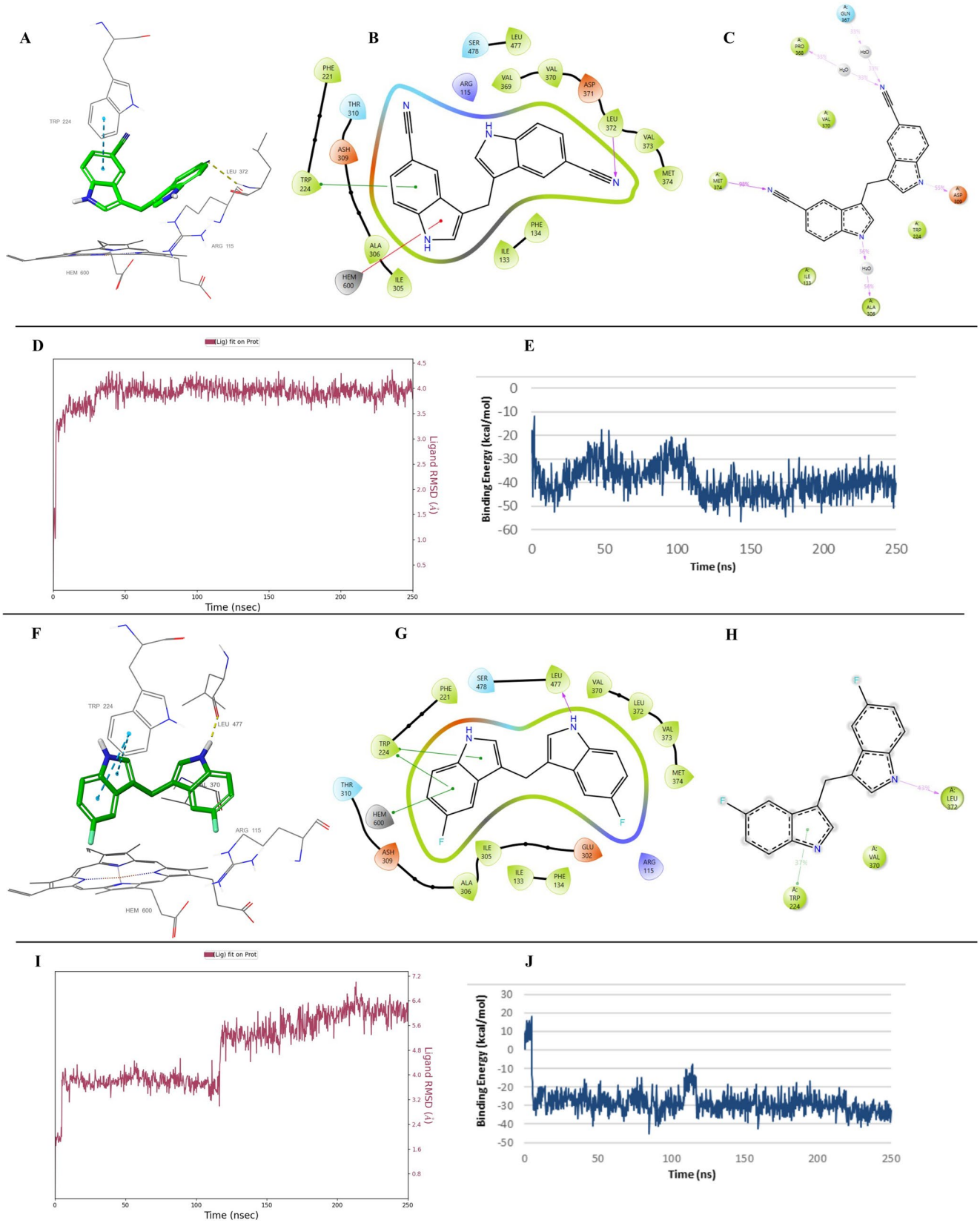
A
TRP 224
LEU 372
ARG 115
HEM 600
B
SER 478
LEU 477
PHE 221
VAL 369
VAL 370
ARG 115
ASP 371
THR 310
LEU 372
ASH 309
VAL 373
TRP 224
MET 374
PHE 134
ILE 133
ALA 306
HEM 600
ILE 305
C
D
(Lig) fit on Prot
Ligand RMSD (Å)
Time (nsec)
E
Binding Energy (kcal/mol)
Time (ns)
F
TRP 224
LEU 477
ARG 115
HEM 600
G
SER 478
LEU 477
VAL 370
PHE 221
LEU 372
VAL 373
TRP 224
MET 374
THR 310
HEM 600
ASH 309
ILE 305
GLU 302
ARG 115
ILE 133
PHE 134
ALA 306
H
I
(Lig) fit on Prot
Ligand RMSD (Å)
Time (nsec)
J
Binding Energy (kcal/mol)
Time (ns)

Fig. 4 Molecular modelling results of compounds X2 (A, B,C, D,E) and X5 (F, G,H, I,J) with CYP19A1. **A**, **F**: The docked pose of compounds in the binding pocket of CYP19A1 (PDB entry: 3S79). Hydrogen bonds are indicated in yellow dashed lines and halogen bonds are indicated in pink dashed lines. **B**, **G**: 2D overview of the docked pose of the ligand in the binding pocket. The hydrogen bond is indicated with a pink arrow and the halogen bond is indicated with a yellow arrow. Hydrophobic amino acids are indicated in green, negatively charged amino acids are indicated in red, positively charged amino acids are indicated in purple and polar amino acids are indicated in blue. **C**, **H**: The binding interactions during the 250 ns MD simulation. The interactions present for at least 30% of the MD simulation are shown. Hydrogen bonds are indicated in pink lines. **D**, **I**: The RMSD of the ligand. **E**, **J**: The MM-GBSA protein-ligand interaction energy (kcal/mol) during the MD simulation

Phe134 (67% of the simulation time). The other indole rings preserved interaction with Phe231 (43% of the simulation time) also A hydrogen bond with Asn228 (33% of the simulation time) and via a bridging water molecule. The nitrile group interact to the same indole ring was observed to form water-mediated hydrogen bonds with Ser127 (67% of the simulation time) and Asn265 (68% of the simulation time). On the other hand, the other nitrile group was observed to form a water-mediated hydrogen bond with Ile399 (45% of simulation time). Asp326 (36% of simulation time) formed a direct hydrogen bond with the nitrogen atom (Fig. 5C). The MM/GBSA binding energy (kcal/mol) was mainly between −20 and −40 kcal/mol with an average binding energy was −25,1332 +/- 7,8587 kcal/mol (Fig. 5E).

The docked pose of X5 showed that one of the indole rings was located close to the heme group and formed hydrophobic interactions while its amine group formed a hydrogen bond with the side chain of Asp333 (Fig. 5F, G). The other indole ring formed π-π stackings with the sidechain of Phe231 and a hydrogen bond with the sidechain of Ser127. An aromatic hydrogen bond with the sidechain of Asp326 was also observed. During the MD simulation the ligand's RMSD value increased towards approximately 5–6 Å (Fig. 5I), indicating a change in binding interactions. One of the indole rings formed a hydrogen bond with Asp333 (31% of the simulation time) (Fig. 5H). In addition, it adopted π-π interactions with the sidechain of Phe231 (56% of the simulation time), formerly an interaction observed with the other indole ring. Also, a hydrogen bonded with Asn228 via a bridging water molecule (43% of the simulation time). The second indole ring formed π-π stackings with the sidechain of Phe268 and hydrophobic interactions with Leu225. The MM/GBSA binding energy (kcal/mol) was mainly between −40 and −60 kcal/mol with an average binding energy was −45.5571+/- 4,6676 kcal/mol (Fig. 5J).

Molecular modelling studies have been performed to suggest binding interactions of compounds X2 and X5 with CYP19A1 and CYP1B1. Among the tested derivatives, X2 emerged as the most potent, showing significant inhibition of both aromatase and CYP1B1, key enzymes involved in estrogen metabolism and genotoxicity. The results suggest that the ligands may adopt multiple binding modes and diverse interactions with the binding pockets of the target proteins. This is in line with the architecture of the binding pockets, which contain many hydrophobic and/or aromatic residues, and with the structure of the investigated ligands, which have aromatic groups as well as hydrogen bonding features. The favorable binding profiles predicted for X2 and X5 are consistent with their experimentally observed enzyme inhibitory activities, particularly the potent dual inhibition exhibited by X2. However, these findings provide qualitative mechanistic support and should not be interpreted as a direct quantitative prediction of biological potency.

Conclusion

This study demonstrates the potential of newly synthesized DIM derivatives as multi-target agents against estrogen receptor-positive breast cancer. The compounds exhibited enhanced cytotoxic activity compared to the parent DIM structure, particularly in MCF-7 cells, along with greater cytotoxic activity in breast cancer cells than in normal breast epithelial cells. In addition to their antiproliferative effects, the derivatives effectively inhibited aromatase and CYP1B1, key enzymes involved in estrogen biosynthesis and metabolism, and reduced cancer cell migration, supporting their potential as multi-target modulators of estrogen-related pathways involved in tumor progression. Molecular modelling studies further supported these findings by revealing favorable interactions of the compounds within hydrophobic binding pockets, including hydrogen bonding and π–π stacking interactions, which may contribute to their biological activity. The SwissADME analysis indicated that the DIM derivatives possess favorable drug-like properties, including high gastrointestinal absorption, balanced lipophilicity, and compliance with Lipinski's rule of five. Their predicted CYP interaction profiles further support their multi-target potential, consistent with the observed biological activities.

Although the cytotoxic potency of the derivatives remains lower than that of conventional chemotherapeutics such as paclitaxel, their selective and multi-target profiles suggest that they may serve as promising candidates for adjuvant or combination therapies. Future studies should focus on structure–activity relationship optimization and further pharmacological evaluation to enhance their efficacy and therapeutic potential.

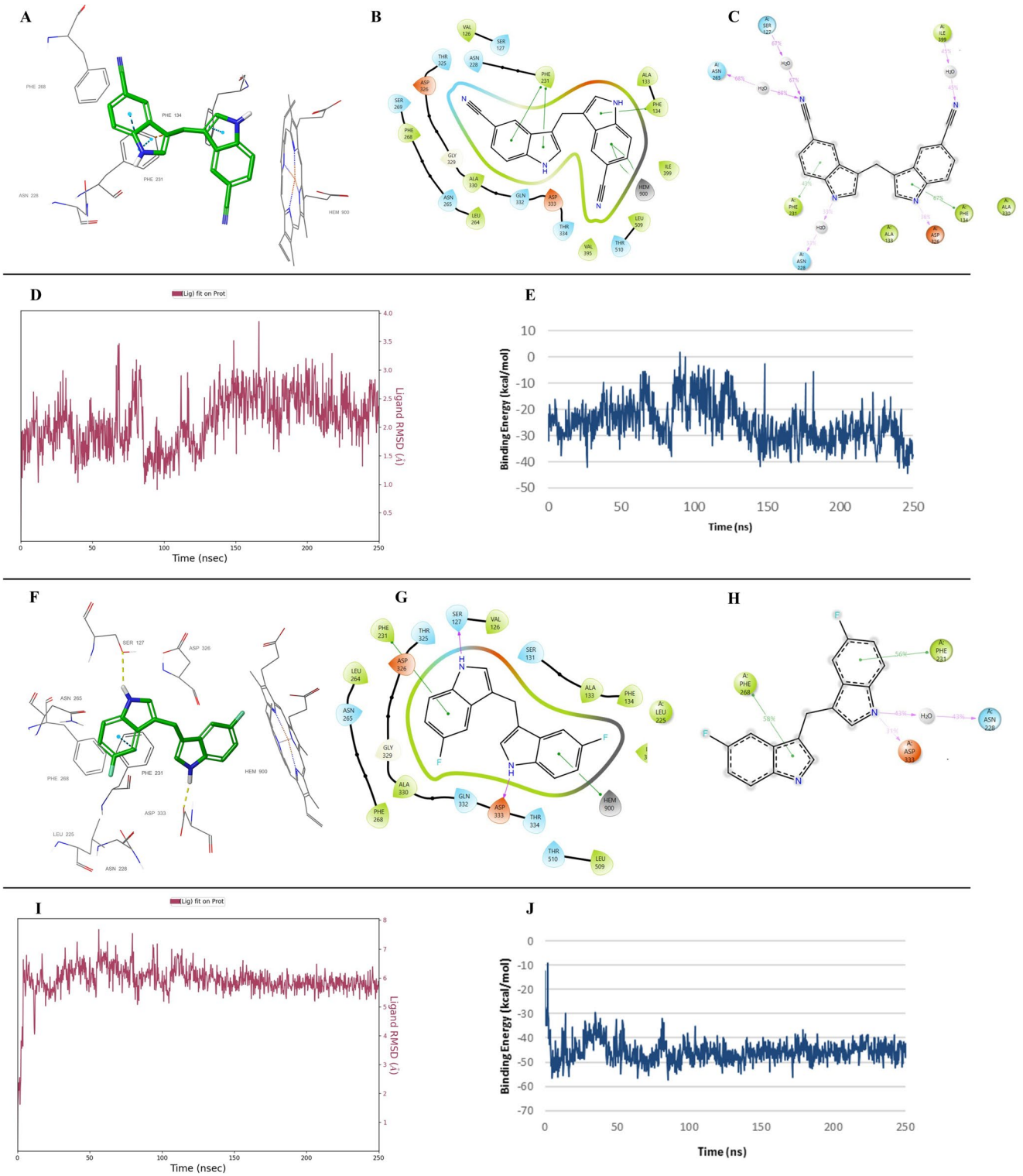

Fig. 5 Molecular modelling results of compounds X2 (A, B,C, D,E) and X5 (F, G,H, I,J) with CYP1B1. **A**, **F**: The docked pose of compounds in the binding pocket of CYP1B1 (PDB entry: 3PM0). Hydrogen bonds are indicated in yellow dashed lines and halogen bonds are indicated in pink dashed lines. **B**, **G**: 2D overview of the docked pose of the ligand in the binding pocket. The hydrogen bond is indicated with a pink arrow and the halogen bond is indicated with a yellow arrow. Hydrophobic amino acids are indicated in green, negatively charged amino acids are indicated in red, positively charged amino acids are indicated in purple and polar amino acids are indicated in blue. **C**, **H**: The binding interactions during the 250 ns MD simulation. The interactions present for at least 30% of the MD simulation are shown. Hydrogen bonds are indicated in pink lines. **D**, **I**: The RMSD of the ligand. **E**, **J**: The MM-GBSA protein-ligand interaction energy (kcal/mol) during the MD simulation

Supplementary Information The online version contains supplementary material available at https://doi.org/10.1007/s40199-026-00625-x.

Acknowledgements The authors are thankful to Scientific and Technological Research Council of Türkiye (TÜBİTAK) for supporting this research with grant #117S065. Biological activity measurements were performed at Ege University, Faculty of Pharmacy, Pharmaceutical Sciences Research Center (FABAL).

Author contributions EIE: Conceptualization, in vitro studies, formal analysis, writing original draft. BE: in vitro studies, formal analysis, writing original draft. HS: Synthesis and characterization of the compounds. SS: Synthesis and characterization of the compounds, review and editing of the original draft, and supervision. AA: Molecular modelling studies, formal analysis, review and editing of the original draft. OE: molecular modelling studies, formal analysis, writing original draft. HGO: Conceptualization, review and editing of the original draft, supervision, and funding acquisition.

Funding This work was supported by the Scientific and Technological Research Council of Türkiye (TÜBİTAK) under Grant No. 117S065.

Data availability The data that support the findings of this study are not openly available due to reasons of sensitivity and are available from the corresponding author upon reasonable request.

Declarations

Competing interests The authors declare no competing interests.

References

1. Al-Shami K, Awadi S, Khamees A, Alsheikh AM, Al-Sharif S, Ala' Bereshy R, Al-Eitan SF, Banikhaled SH, Al-Qudimat AR, Al-Zoubi RM. Al Zoubi, Estrogens and the risk of breast cancer: A narrative review of literature. Heliyon. 2023;9:e20224. https://doi.org/10.1016/j.heliyon.2023.e20224.
2. Lecarpentier J, Noguès C, Mouret-Fourme E, Buecher B, Gauthier-Villars M, Stoppa-Lyonnet D, Bonadona V, Fricker JP, Berthet P, Caron O, Coupier I, Pujol P, Faivre L, Gesta P, Eisinger F, Mari V, Gladieff L, Lortholary A, Luporsi E, Leroux D, Venat-Bouvet L, Maugard CM, Colas C, Tinat J, Lasset C, Andrieu N. Breast cancer risk associated with estrogen exposure and truncating mutation location in BRCA1/2 carriers, Cancer Epidemiol. Biomarkers Prev. 2015;24:698–707. https://doi.org/10.1158/1055-9965.EPI-14-0884.
3. Yager JD. Mechanisms of estrogen carcinogenesis: The role of E2/E1–quinone metabolites suggests new approaches to preventive intervention – A review. Steroids. 2015;99:56–60. https://doi.org/10.1016/j.steroids.2014.08.006.
4. Yue W, Yager JD, Wang JP, Jupe ER, Santen RJ. Estrogen receptor-dependent and independent mechanisms of breast cancer carcinogenesis. Steroids. 2013;78:161–70. https://doi.org/10.1016/j.steroids.2012.11.001.
5. Schuster EF, Lopez-Knowles E, Alataki A, Zabaglo L, Folkerd E, Evans D, Sidhu K, Cheang MCU, Tovey H, Salto-Tellez M, Maxwell P, Robertson J, Smith I, Bliss JM, Dowsett M. Molecular profiling of aromatase inhibitor sensitive and resistant ER+HER2- postmenopausal breast cancers. Nat Commun. 2023;14. https://doi.org/10.1038/s41467-023-39613-z.
6. Rani S, Raheja K, Luxami V, Paul K. A review on diverse heterocyclic compounds as the privileged scaffolds in non-steroidal aromatase inhibitors. Bioorg Chem. 2021;113. https://doi.org/10.1016/j.bioorg.2021.105017.
7. Williams DE. Indoles derived from glucobrassicin: Cancer chemoprevention by indole-3-carbinol and 3,3′-diindolylmethane. Front Nutr. 2021;8. https://doi.org/10.3389/fnut.2021.734334.
8. Kaiser AE, Baniasadi M, Giansiracusa D, Giansiracusa M, Garcia M, Fryda Z, Wong TL, Bishayee A. Sulforaphane: A broccoli bioactive phytocompound with cancer preventive potential. Cancers (Basel). 2021;13. https://doi.org/10.3390/cancers13194796.
9. Verschoyle RD, Steward WP, Gescher AJ. Putative cancer chemopreventive agents of dietary origin - How safe are they? Nutr Cancer. 2007;59:152–62. https://doi.org/10.1080/01635580701458186.
10. Zhou Q, Wang Y, Han X, Fu S, Zhu C, Chen Q. Efficacy of resveratrol supplementation on glucose and lipid metabolism: A meta-analysis and systematic review. Front Physiol. 2022;13:795980. https://doi.org/10.3389/fphys.2022.795980.
11. He H, Ma Y, Huang H, Huang C, Chen Z, Chen D, Gu Y, Wang X, Chen J. A comprehensive understanding about the pharmacological effect of diallyl disulfide other than its anti-carcinogenic activities. Eur J Pharmacol. 2021;893:173803. https://doi.org/10.1016/j.ejphar.2020.173803.
12. Qian J, Xu Z, Zhu P, Meng C, Liu Y, Shan W, He A, Gu Y, Ran F, Zhang Y, Ling Y. A derivative of piperlongumine and ligustrazine as a potential thioredoxin reductase inhibitor in drug-resistant hepatocellular carcinoma. J Nat Prod. 2021;84:3161–8. https://doi.org/10.1021/acs.jnatprod.1c00618.
13. Ji P, Wang X, Yin J, Mou Y, Huang H, Ren Z. Selective delivery of curcumin to breast cancer cells by self-targeting apoferritin nanocages with pH-responsive and low toxicity. Drug Deliv. 2022;29:986–96. https://doi.org/10.1080/10717544.2022.2056662.
14. Dash R, Hosen SMZ, Karim MR, Kabir MSH, Hossain MM, Junaid M, Islam A, Paul A, Khan MA. In silico analysis of indole-3-carbinol and its metabolite DIM as EGFR tyrosine kinase inhibitors in platinum resistant ovarian cancer vis a vis ADME/T property analysis. J Appl Pharm Sci. 2015;5:073–8. https://doi.org/10.7324/JAPS.2015.501112.
15. Mitra S, Dash R. Natural products for the management and prevention of breast cancer, Evid.-Based Complement. Altern. Med. 2018 (2018). https://doi.org/10.1155/2018/8324696
16. Penta D, Tripathi P, Rajarajan D, Natesh J, Mondal P, Meeran SM. Diindolylmethane promotes metabolic crisis and enhances the efficacy of centchroman in breast cancer: A 1H NMR-based approach. ACS Omega. 2022;7:43147–60. https://doi.org/10.1021/acsomega.2c05832.
17. Singh S, Gupta N, Mishra DP, Verma S. Diindolylmethane-containing peptides inhibit invasion and epithelial-mesenchymal transition-associated gene expression in hormone-dependent breast cancer. Bioorg Med Chem. 2026;132:118421. https://doi.org/10.1016/j.bmc.2025.118421.
18. Fan S, Meng Q, Saha T, Sarkar FH, Rosen EM. Low concentrations of diindolylmethane, a metabolite of indole-3-carbinol, protect against oxidative stress in a BRCA1-dependent manner. Cancer Res. 2009;69:6083–91. https://doi.org/10.1158/0008-5472.CAN-08-3309.
19. Wang W, Lv M, Wang Y, Zhang J. Development of novel application of 3,3′-diindolylmethane: sensitizing multidrug resistance human breast cancer cells to γ-irradiation. Pharm Biol. 2016;54:3164–8. https://doi.org/10.1080/13880209.2016.1192198.
20. Reyes-Hernández OD, Figueroa-González G, Quintas-Granados LI, Gutiérrez-Ruíz SC, Hernández-Parra H, Romero-Montero A, Del Prado-Audelo ML, Bernal-Chavez SA, Cortés H, Peña-Corona SI, Kiyekbayeva L, Ateşşahin DA, Goloshvili T, Leyva-Gómez G, Sharifi-Rad J. 3,3′-diindolylmethane and

indole-3-carbinol: Potential therapeutic molecules for cancer chemoprevention and treatment via regulating cellular signaling pathways. Cancer Cell Int. 2023;23. https://doi.org/10.1186/s12935-023-03031-4.
21. Thomson CA, Chow HHS, Wertheim BC, Roe DJ, Stopeck A, Maskarinec G, Altbach M, Chalasani P, Huang C, Strom MB, Galons JP, Thompson PA. A randomized, placebo-controlled trial of diindolylmethane for breast cancer biomarker modulation in patients taking tamoxifen. Breast Cancer Res Treat. 2017;165:97–107. https://doi.org/10.1007/s10549-017-4292-7.
22. Anderton MJ, Manson MM, Verschoyle RD, Gescher A, Lamb JH, Farmer PB, Steward WP, Williams ML. Pharmacokinetics and tissue disposition of indole-3-carbinol and its acid condensation products after oral administration to mice. Clin Cancer Res. 2004;10:5233–41. https://doi.org/10.1158/1078-0432.CCR-04-0163.
23. Luo Y, Wang TTY, Teng Z, Chen P, Sun J, Wang Q. Encapsulation of indole-3-carbinol and 3,3′-diindolylmethane in zein/carboxymethyl chitosan nanoparticles with controlled release property and improved stability. Food Chem. 2013;139:224–30. https://doi.org/10.1016/j.foodchem.2013.01.113.
24. Maciejewska D, Rasztawicka M, Wolska I, Anuszewska E, Gruber B. Novel 3,3′-diindolylmethane derivatives: Synthesis and cytotoxicity, structural characterization in solid state. Eur J Med Chem. 2009;44:4136–47. https://doi.org/10.1016/j.ejmech.2009.05.011.
25. Ozcan-Sezer S, Ince E, Akdemir A, Ceylan ÖÖ, Suzen S, Gurer-Orhan H. Aromatase inhibition by 2-methyl indole hydrazone derivatives evaluated via molecular docking and in vitro activity studies. Xenobiotica. 2019;49. https://doi.org/10.1080/00498254.2018.1482029.
26. Burke MD, Mayer RT. Ethoxyresorufin: direct fluorimetric assay of a microsomal O-dealkylation which is preferentially inducible by 3-methylcholanthrene. Drug Metab Dispos. 1974;2:583–8.
27. Soto AM, Sonnenschein C, Chung KL, Fernandez MF, Olea N, Serrano FO. The E-SCREEN assay as a tool to identify estrogens: An update on estrogenic environmental pollutants. Environ Health Perspect. 1995;103:113–22. https://doi.org/10.1289/ehp.95103s7113.
28. Entezari B, Bozdag D, Gurer-Orhan H. Evaluation of endocrine related adverse effects of non-endocrine targeted pharmaceuticals in cellular systems. Endocr Metab Immune Disord Drug Targets. 2023;23:1740–9. https://doi.org/10.2174/1871530323666230224145624.
29. Mosmann T. Rapid colorimetric assay for cellular growth and survival: Application to proliferation and cytotoxicity assays. J Immunol Methods. 1983;65:55–63. https://doi.org/10.1016/0022-1759(83)90303-4.
30. Masetti M, Falchi F, Gioia D, Recanatini M, Ciurli S, Musiani F. Targeting the protein tunnels of the urease accessory complex: A theoretical investigation. Molecules. 2020;25. https://doi.org/10.3390/molecules25122911.
31. Mahmod AI, Haif SK, Kamal A, Al-ataby IA, Talib WH. Chemoprevention effect of the Mediterranean diet on colorectal cancer: Current studies and future prospects. Front Nutr. 2022;9. https://doi.org/10.3389/fnut.2022.924192.
32. Sukprasansap M, Chanvorachote P. Evidence of potential plant-derived compounds with anticancer effects on lung cancer: Clinical and molecular pharmacology approaches. Anticancer Res. 2022;42:4247–58. https://doi.org/10.21873/anticanres.15924.
33. Alharbi KS, Almalki WH, Makeen HA, Albratty M, Meraya AM, Nagraik R, Sharma A, Kumar D, Chellappan DK, Singh SK, Dua K, Gupta G. Role of medicinal plant-derived nutraceuticals as a potential target for the treatment of breast cancer. J Food Biochem. 2022;46. https://doi.org/10.1111/jfbc.14387.
34. Kulkarni M, Hussain MA, Valdar RS, Hebbar S, Laha S. Exploring the cancer therapeutic potential of traditional medicinal plants by modulating the apoptotic pathway, Biomed. Res. Int. 2026 (2026). https://doi.org/10.1155/BMRI/2086738
35. Meer N, Elamin A, Mohammed F, Bashir F, Tayyem R. Dietary polyphenols as anticancer agents: A review of recent advances and mechanisms. Nutr Health. 2026;32. https://doi.org/10.1177/02601060251411197.
36. Mandrich L, Caputo E. Brassicaceae-derived anticancer agents: Towards a green approach to beat cancer. Nutrients. 2020;12:868. https://doi.org/10.3390/nu12030868.
37. Gasmi A, Gasmi Benahmed A, Shanaida M, Chirumbolo S, Menzel A, Anzar W, Arshad M, Cruz-Martins N, Lysiuk R, Beley N, Oliinyk P, Shanaida V, Denys A, Peana M, Bjørklund G. Anticancer activity of broccoli, its organosulfur and polyphenolic compounds. Crit Rev Food Sci Nutr. 2024;64:8054–72. https://doi.org/10.1080/10408398.2023.2195493.
38. Licznerska BE, Szaefer H, Murias M, Bartoszek A, Baer-Dubowska W. Modulation of CYP19 expression by cabbage juices and their active components: Indole-3-carbinol and 3,3′-diindolylmethene in human breast epithelial cell lines. Eur J Nutr. 2013;52:1483–92. https://doi.org/10.1007/s00394-012-0455-9.
39. Wouters W, De Coster R, Goeminne N, Beerens D, van Dun J. Aromatase inhibition by the antifungal ketoconazole. J Steroid Biochem. 1988;30:387–9.
40. Di Matteo M, Ammazzalorso A, Andreoli F, Caffa I, De Filippis B, Fantacuzzi M, Giampietro L, Maccallini C, Nencioni A, Parenti MD, Soncini D, Del Rio A, Amoroso R. Synthesis and biological characterization of 3-(imidazol-1-ylmethyl) piperidine sulfonamides as aromatase inhibitors. Bioorg Med Chem Lett. 2016;26:3192–4. https://doi.org/10.1016/j.bmcl.2016.04.078.
41. Zhao M, Ma J, Li M, Zhang Y, Jiang B, Zhao X, Huai C, Shen L, Zhang N, He L, Qin S. Cytochrome P450 enzymes and drug metabolism in humans. Int J Mol Sci. 2021;22. https://doi.org/10.3390/ijms222312808.
42. Tokizane T, Shiina H, Igawa M, Enokida H, Urakami S, Kawakami T, Ogishima T, Okino ST, Li LC, Tanaka Y, Nonomura N, Okuyama A, Dahiya R. Cytochrome P450 1B1 is overexpressed and regulated by hypomethylation in prostate cancer, Clin. Cancer Res. 2005;11:5793–801. https://doi.org/10.1158/1078-0432.CCR-04-2545.
43. McKay JA, Melvin WT, Ah-See AK, Ewen SWB, Greenlee WF, Marcus CB, Burke MD, Murray GI. Expression of cytochrome P450 CYP1B1 in breast cancer. FEBS Lett. 1995;374:270–2. https://doi.org/10.1016/0014-5793(95)01126-Y.
44. Kwon YJ, Baek HS, Ye DJ, Shin S, Kim D, Chun YJ. CYP1B1 enhances cell proliferation and metastasis through induction of EMT and activation of Wnt/β-catenin signaling via Sp1 upregulation. PLoS One. 2016;11. https://doi.org/10.1371/journal.pone.0151598.
45. Giudice A, Barbieri A, Bimonte S, Cascella M, Cuomo A, Crispo A, D'arena G, Galdiero M, Della Pepa ME, Botti G, Caraglia M, Capunzo M, Arra C, Montella M. Dissecting the prevention of estrogen-dependent breast carcinogenesis through Nrf2-dependent and independent mechanisms, Onco. Targets Ther. 2019;12:4937–53. https://doi.org/10.2147/OTT.S183192.
46. Dutour R, Poirier D. Inhibitors of cytochrome P450 (CYP) 1B1, Eur. J Med Chem. 2017;135:296–306. https://doi.org/10.1016/j.ejmech.2017.04.042.
47. Szaefer H, Licznerska B, Krajka-Kuniak V, Bartoszek A, Baer-Dubowska W. Modulation of CYP1A1, CYP1A2 and CYP1B1 expression by cabbage juices and indoles in human breast cell lines. Nutr Cancer. 2012;64:879–88. https://doi.org/10.1080/01635581.2012.690928.
48. Nouriemamzaden F, Word B, Cotton E, Hawkins A, Littlejohn K, Moore R, Miranda-Carbon G, Orish CN, Lyn-Cook B. Modulation of estrogen α and progesterone receptors in triple negative breast cancer cell lines: The effects of vorinostat and

indole-3-carbinol in vitro. Anticancer Res. 2020;40:3669–83. https://doi.org/10.21873/anticanres.14356.
49. Marques M, Laflamme L, Benassou I, Cissokho C, Guillemette B, Gaudreau L. Low levels of 3,3′-diindolylmethane activate estrogen receptor α and induce proliferation of breast cancer cells in the absence of estradiol. BMC Cancer. 2014;14. https://doi.org/10.1186/1471-2407-14-524.
50. Caruso JA, Campana R, Wei C, Su CH, Hanks AM, Bornmann WG, Keyomarsi K. Indole-3-carbinol and its N-alkoxy derivatives preferentially target ERα-positive breast cancer cells. Cell Cycle. 2014;13:2587–99. https://doi.org/10.4161/15384101.2015.942210.
51. Shilpa G, Lakshmi S, Jamsheena V, Lankalapalli RS, Prakash V, Anbumani S, Priya S. Studies on the mode of action of synthetic diindolylmethane derivatives against triple negative breast cancer cells, Basic Clin. Pharmacol Toxicol. 2022;131:224–40. https://doi.org/10.1111/bcpt.13767.
52. Draz H, Goldberg AA, Titorenko VI, Tomlinson Guns ES, Safe SH, Sanderson JT. Diindolylmethane and its halogenated derivatives induce protective autophagy in human prostate cancer cells via induction of the oncogenic protein AEG-1 and activation of AMP-activated protein kinase (AMPK). Cell Signal. 2017;40:172–82. https://doi.org/10.1016/j.cellsig.2017.09.006.
53. Dong J, Wang Z, Meng Q, Zhang Q, Huang G, Cui J, Li S. Development of 2-arylbenzo[h]quinolone analogs as selective CYP1B1 inhibitors. RSC Adv. 2018;8:15009–20. https://doi.org/10.1039/C8RA00465J.
54. Dong J, Zhang Q, Cui Q, Huang G, Pan X, Li S. Flavonoids and naphthoflavonoids: Wider roles in the modulation of cytochrome P450 family 1 enzymes. ChemMedChem. 2016;11:2102–18. https://doi.org/10.1002/cmdc.201600316.